Turkish Journal of Remote Sensing and GIS
Türk Uzaktan Algılama ve CBS Dergisi

Turk J Remote Sens GIS, March 2026, 7(1): 145–165
Journal homepage: http://www.dergipark.org.tr/en/pub/rsgis

Assessing Burned Area and Severity in Mediterranean Forests Using Bi-Temporal Sentinel-2 and CORINE Data: The Manavgat 2021 Wildfire Case

Akdeniz Ormanlarında Yanık Alan ve Şiddetinin Bi-Temporal Sentinel-2 ve CORINE Verileri Kullanılarak Değerlendirilmesi: Manavgat 2021 Orman Yangını Örneği

Melih Altay[1]*, Mustafa Türker[1]

[1]*Hacettepe University, Faculty of Engineering, Department of Geomatics Engineering, Çankaya, Ankara/Türkiye.*

ORIGINAL PAPER

***Corresponding author:**
Melih Altay
melihaltay17@hacettepe.edu.tr

doi: 10.48123/rsgis.1775666

Article history
Received: 01.09.2025
Accepted: 04.12.2025
Published: 26.03.2026

Abstract

In this study, burned forest areas were identified using bi-temporal Sentinel-2 imagery acquired before and after the fire, through the application of spectral indices such as the Normalized Burn Ratio (NBR) and the Normalized Difference Vegetation Index (NDVI). Specifically, the forest fire that occurred in the Manavgat district of Antalya Province, Türkiye, on July 27, 2021, was analyzed based on NBR and NDVI values derived from Sentinel-2 satellite data. The Normalized Burn Ratio (NBR) variants NBR1 and NBR2, and NDVI indexes were evaluated comparatively. To reduce confusion between agricultural areas and burnt forest regions we excluded agricultural fields from processing through using the CORINE land cover database. The achieved results showed that the NDVI-based detection provided the highest overall accuracy (OA) of 97.1% and a Kappa of 0.950, while NBR2 and NBR1 resulted in OA values of 96.8% and 96.3%, respectively. The high NDVI performance is primarily attributed to the mixed forest–cropland mosaic structure of the study area, which enhances spectral contrast between burned and unburned surfaces. Masking agricultural areas with the existing CORINE database reduced the false positives and hence improved detection reliability for all indexes. The results demonstrated that the used methodology has high effectiveness in quantitatively mapping fire damages and supporting rehabilitation planning.

Keywords: *Forest fire, Sentinel-2, Bi-temporal analysis, Spectral indices*

Özet

Bu çalışmada yanmış orman alanları, yangın öncesinde ve sonrasında toplanan iki zamanlı Sentinel-2 uydu görüntülerini kullanarak, Normalize Yanma Oranı (NBR) ve Normalize Fark Bitki Örtüsü Endeksi (NDVI) gibi spektral indeksler kullanılarak tespit edilmiştir. Özellikle, 27 Temmuz 2021 tarihinde Türkiye'nin Antalya ilinin Manavgat ilçesinde meydana gelen orman yangını, Sentinel-2 uydu verilerinden elde edilen NBR ve NDVI değerleri temelinde analiz edildi. Normalleştirilmiş Yanma Oranı (NBR) varyantları NBR1 ve NBR2 ile NDVI indeksleri karşılaştırmalı olarak değerlendirilmiştir. Tarımsal alanlar ile yanmış orman bölgeleri arasındaki karışıklığı azaltmak için, CORINE arazi örtüsü veritabanını kullanarak tarımsal alanları işlemden hariç tuttuk. Elde edilen sonuçlar, NDVI tabanlı algılamanın 97,1% ile en yüksek genel doğruluk (OA) ve 0,950 Kappa değeri sağladığını, NBR2 ve NBR1'in ise sırasıyla 96,8% ve 96,3% OA değerleri sağladığını göstermiştir. NDVI'nın yüksek performansı, öncelikle çalışma alanının karışık orman-tarım arazisi mozaik yapısına atfedilebilir; bu yapı, yanmış ve yanmamış yüzeyler arasındaki spektral kontrastı artırmaktadır. Mevcut CORINE veritabanı ile tarım alanlarının maskelenmesi, yanlış pozitifleri azaltmış ve dolayısıyla tüm endeksler için algılama güvenilirliğini artırmıştır. Sonuçlar, kullanılan metodolojinin yangın hasarlarını nicel olarak haritalandırmada ve rehabilitasyon planlamasını desteklemede yüksek etkinliğe sahip olduğunu göstermiştir.

Anahtar kelimeler: *Orman yangını, Sentinel-2, İki zamanlı analiz, Spektral indeks*

1. Introduction

Forests over approximately one-third of Earth's land surface and provide vital ecosystem services including carbon storage, water regulation, soil protection, and climate moderation (International Union for Conservation of Nature, 2022; U.S. Department of Agriculture, 2023). Containing 70–90% of terrestrial biomass, forests are essential for biodiversity conservation and climate stability, serving as habitat for nearly 80% of terrestrial species and contributing significantly to global carbon sequestration (Reichstein et al., 2019; Wilson et al., 1988). However, these ecosystems face unprecedented threats from wildfires, which have emerged as one of the most pressing environmental challenges of the 21st century (Jolly et al., 2015). Climate change has fundamentally altered global fire regimes, creating conditions characterized by prolonged droughts, elevated temperatures, and extended fire seasons (Abatzoglou & Williams, 2016; Flannigan et al., 2009; Turco et al., 2018). As a result, millions of hectares are destroyed annually by fires triggered by both natural and anthropogenic causes, disrupting ecosystems, accelerating biodiversity decline, and intensifying global warming through increased carbon emissions (Park et al., 2023; Younger et al., 2024; Wang et al., 2025; NASA, 2025).

The ecological consequences of wildfires extend beyond vegetation loss, including soil erosion, hydrological cycle disruption, and long-term ecosystem degradation. These impacts vary depending on fire intensity, fuel load, and ecosystem characteristics, making rapid and accurate post-fire mapping essential for damage assessment, ecological rehabilitation, and risk reduction (Chuvieco et al., 2019). Traditional ground surveys are time-intensive and costly, whereas satellite-based remote sensing provides efficient and large-scale alternatives. Technologies such as Synthetic Aperture Radar (SAR) and multispectral imaging offer multi-temporal capabilities, enabling fire spread monitoring and severity assessment even under challenging conditions like smoke or cloud cover (Chen et al., 2017). Among these, Sentinel-2 imagery has proven particularly effective due to its high spatial resolution, frequent revisit cycle, and multispectral capabilities (Drusch et al., 2012), and has been widely applied for burned area detection, severity mapping, and post-fire vegetation recovery using both spectral indices and machine learning approaches (Gibson et al., 2020; Yılmaz et al., 2023; Gündüz et al., 2025).

Spectral indices remain central to wildfire monitoring due to their simplicity and robustness. The Normalized Burn Ratio (NBR) is widely employed for burned area detection and severity assessment (Bannari, 2009; Key & Benson, 2006), with refinements such as the differenced NBR (dNBR), Relativized dNBR (RdNBR), and Relativized Burn Ratio (RBR) providing improved severity quantification (Miller & Thode, 2007; Parks et al., 2014). Complementary indices like the Normalized Difference Water Index (NDWI) and Burned Area Index (BAI) further enhance discrimination in fire-affected landscapes (Veraverbeke et al., 2012; Chuvieco et al., 2019). Recent research increasingly emphasizes multi-platform approaches that integrate Sentinel-2 with MODIS, Landsat, SAR, LiDAR, and hyperspectral data, while advanced methods such as adaptive thresholding and unsupervised classification improve accuracy in heterogeneous Mediterranean landscapes.

The Mediterranean basin faces unique wildfire management challenges due to its hot, dry summers and complex mosaic of forests, croplands, and urban development (Pausas et al., 2008; Moreira et al., 2011). Turkey, as a critical part of this region, is particularly vulnerable given its diverse topography and rapidly expanding wildland–urban interface (Türkeş & Altan, 2008). The catastrophic 2021 wildfires in southern Turkey underscored the urgent need for improved monitoring systems and rapid assessment capabilities (Almeida et al., 2023). Although satellite-based burned area mapping techniques are widely applied globally including CORINE-based approaches in European contexts—no systematic evaluation has been conducted for Turkish Mediterranean forest ecosystems (Franquesa et al., 2018). This represents a significant gap given Turkey's unique geographical and ecological conditions, which may require tailored approaches. Despite the global advancement in burned area mapping, no comprehensive assessment has yet been conducted for Turkish Mediterranean ecosystems using Sentinel-2 data, representing a critical knowledge gap addressed by this study.

Accordingly, this study aims to evaluate the effectiveness of bi-temporal Sentinel-2 imagery for burned area detection in Mediterranean forests using spectral indices including NDVI, NBR1, and NBR2. The specific objectives are: (1) to compare the accuracy and performance of different spectral indices for burned area classification, (2) to integrate CORINE land cover data in order to minimize misclassification of agricultural lands, and (3) to establish a robust methodological framework for operational burned area mapping applicable to Turkish Mediterranean ecosystems. The catastrophic 2021 Manavgat wildfire is adopted as a case study to validate the methodology and provide practical insights into wildfire impacts in one of Turkey's most ecologically and economically significant regions. To the best of our knowledge, this research provides the first systematic accuracy comparison of NDVI, NBR1, and NBR2 for burned area mapping in Türkiye, offering a nationally focused evaluation of index performance.

2. Study Area and Data

2.1 Study Area

The Manavgat district of Antalya Province in Türkiye is located at approximately 36.7875° N latitude and 31.4434° E longitude. Manavgat was exposed to large-scale forest fires during the summer of 2021. These fires significantly affected the ecosystem and structure of the region, threatening the safety of both local residents and tourists. The fires that began on July 27, 2021, first showed their impact in the forested areas west of Manavgat and rapidly spread eastward. The areas where the fires intensified were the forested regions consisting of maquis, Pinus brutia (Turkish pine), Pinus pinea (Stone pine), Quercus coccifera (Kermes oak), and Ceratonia siliqua (Carob tree), particularly surrounding the Oymapınar Dam in the northwest (Aksoy et al., 2024). The impact of the fires caused significant changes in the structural and biodiversity characteristics of the region. This event left permanent marks on local flora and fauna and also caused serious economic damage to the agriculture and tourism sectors. Citrus orchards and olive groves, which are economically important to the region, were among the most affected agricultural lands. Figure 1 shows the study area and the regions affected by the fires.

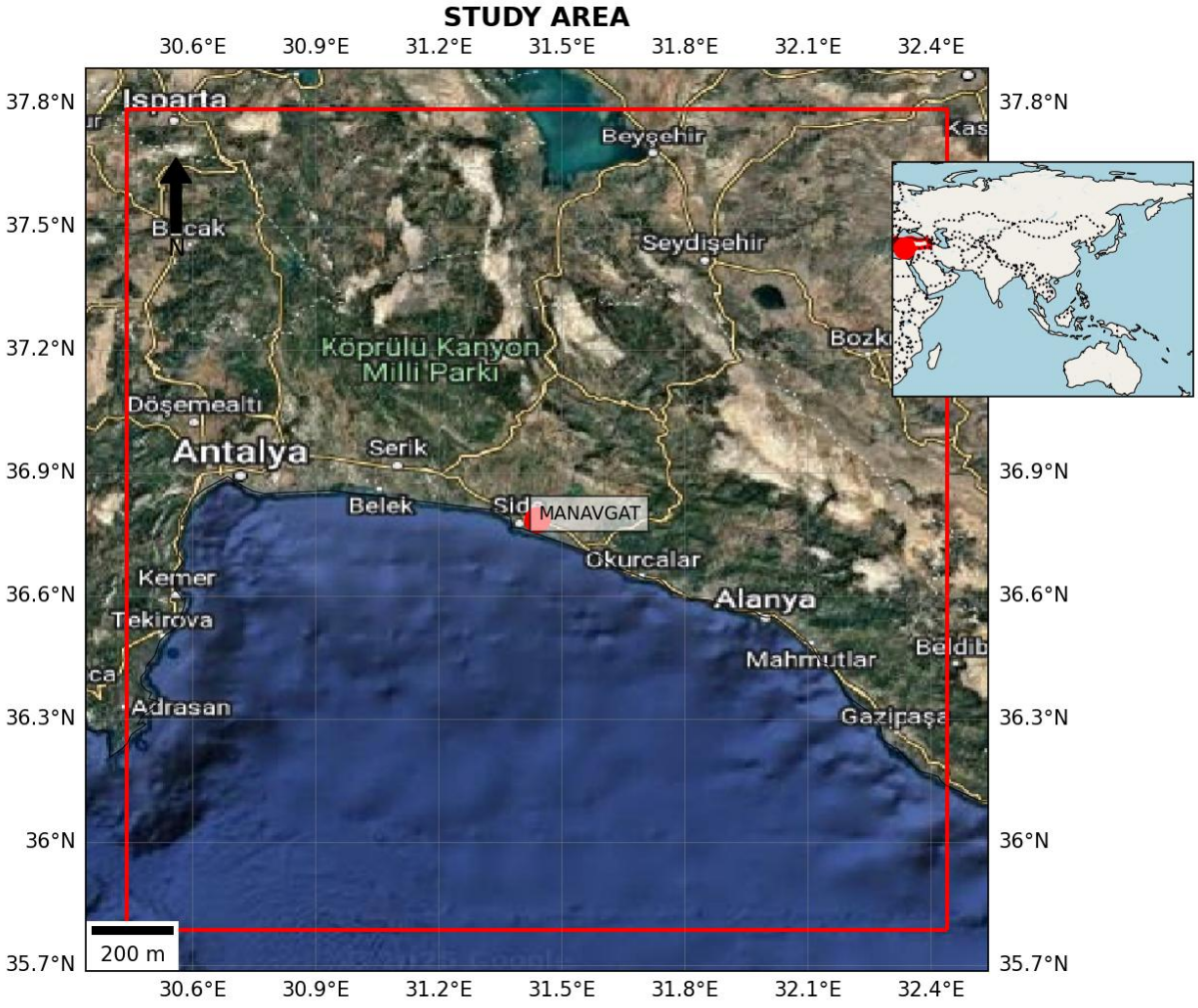

Figure 1. Study area

2.2 Data

The Sentinel-2 mission, developed by the European Space Agency (ESA) within the framework of the Copernicus Programme, represents a cornerstone of global Earth observation infrastructure. The constellation currently comprises Sentinel-2A (launched in June 2015), Sentinel-2B (March 2017), and Sentinel-2C (September 2024), each equipped with a 13-band multispectral imager providing spatial resolutions of 10, 20, and 60 m (Drusch et al., 2012; Li & Roy, 2017;

European Space Agency, 2021). With its high temporal resolution (five-day revisit at the equator), wide swath coverage (~290 km), and broad spectral range covering the visible (VIS), near-infrared (NIR), and short-wave infrared (SWIR) domains, Sentinel-2 has become indispensable in diverse applications including agriculture, forestry, coastal monitoring, land use/land cover change, and disaster management (Chuvieco et al., 2009). In particular, the SWIR bands are highly sensitive to vegetation moisture and structural changes, making them especially effective for discriminating between burned and unburned areas in wildfire studies (Key & Benson, 2006; Miller & Thode, 2007).

In this study, Sentinel-2 Level-2A surface reflectance products were employed to assess pre- and post-fire conditions of the study area. Images acquired on July 20, 2021, and September 3, 2021, were selected to represent pre-fire and post-fire conditions, respectively. The seven-day interval between the pre-fire acquisition and fire onset ensured capture of baseline vegetation conditions without interference from seasonal phenological changes. Level-2A data, corrected for atmospheric effects through the Sen2Cor processor, are particularly suitable for change detection as they reduce atmospheric variability between acquisition dates. Cloud and cloud shadows were masked using the Sentinel-2 Scene Classification (SCL) layer, where pixels classified as clouds, cirrus, cloud shadows, and snow/ice were excluded. In addition, topographic correction (default setting) and ESA-provided orthorectification were applied to ensure geometric accuracy. To further refine geometric consistency, post-fire images were co-registered to pre-fire images with the root mean square (RMS) errors below 0.5 pixels. Figure 2 illustrates the pre-fire (a) and post-fire (b) Sentinel-2 images of the study area. The spectral band characteristics of Sentinel-2 are summarized in Table 1.

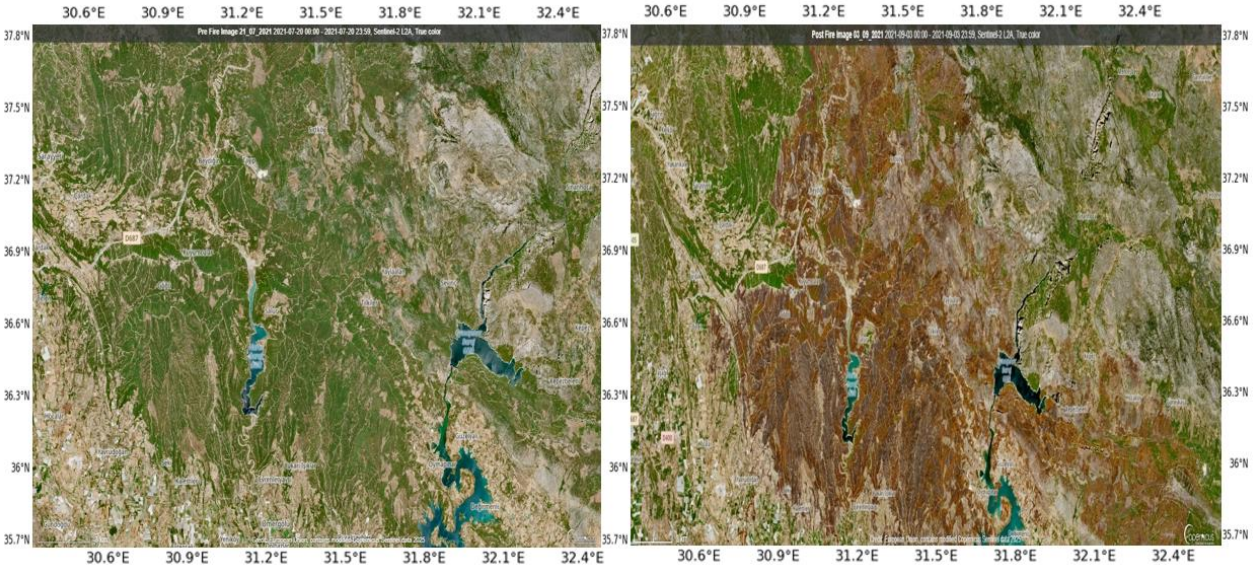

Figure 2. Sentinel-2 MSI images: pre fire (left), post fire (right)

Table 1. Sentinel-2 MSI spectral bands

Spectral Bands	Bands Range (nm)	Spatial Resolution (m)
B1 Coastal/Aerosol	433 – 453	60
B2 Blue	458 – 523	10
B3 Green	560	10
B4 Red	665	10
B5 Red Edge 1	705	20
B6 Red Edge 2	740	20
B7 Red Edge 3	783	20
B8 Near-Infrared (NIR)	842	10
B8A Near-Infrared (Narrow)	865	20
B9 Water Vapour	945	60
B10 SWIR- Cirrus	1375	60
B11 SWIR	1610	20
B12 SWIR	2190	20

3. Methodology

The workflow was structured to ensure clear methodological progression from preprocessing to accuracy validation, as outlined in Figure 3. The methodology was designed as a multi-stage process encompassing data preprocessing, spectral index calculation, burned area detection, burn severity mapping, and accuracy assessment. In the first stage, Sentinel-2 Level-2A imagery was generated using the Sen2Cor atmospheric correction processor, ensuring surface reflectance products. Undesirable pixels, such as clouds and cloud shadows were masked using the Scene Classification Layer (SCL). To guarantee geometric consistency, post-fire images were co-registered to pre-fire scenes, with alignment accuracy controlled to a root mean square error (RMS) below 0.5 pixels.

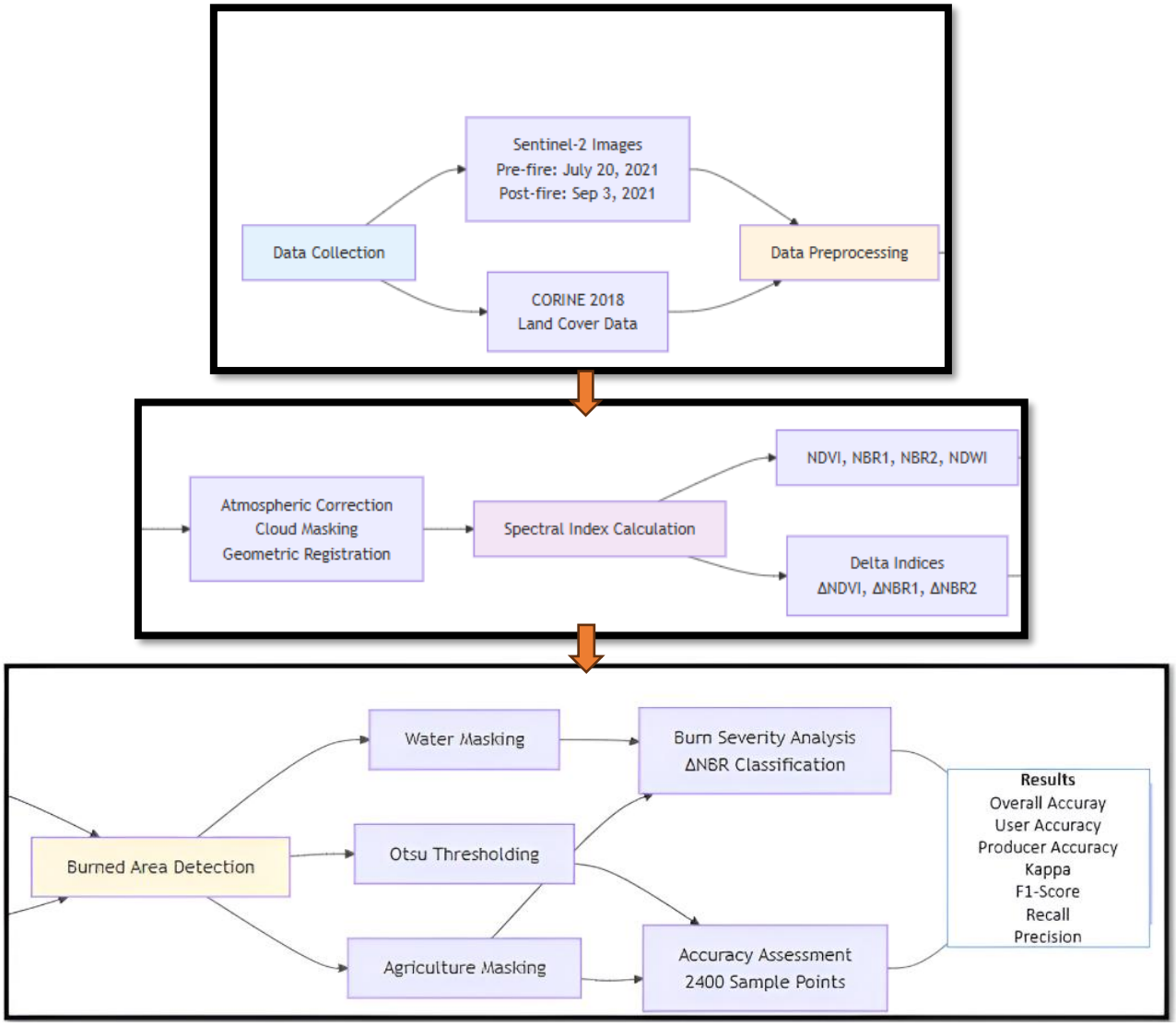

Figure 3. Workflow of study

Following preprocessing, spectral indices sensitive to vegetation and fire-induced changes were computed. Specifically, the Normalized Difference Vegetation Index (NDVI), the Normalized Burn Ratio variants (NBR1 and NBR2), and the Normalized Difference Water Index (NDWI) were derived from pre- and post-fire imagery. These indices were selected due to their proven robustness in vegetation and burn detection studies (Chuvieco et al., 2010; Miller & Thode, 2007). While NDVI provides information on vegetation density, NBR1 and NBR2 are particularly sensitive to structural and moisture changes induced by fire, making them suitable for Mediterranean ecosystems prone to sparse vegetation. The temporal differences of these indices (ΔNDVI, ΔNBR1, ΔNBR2) were then calculated to capture fire-driven changes. To reduce error of detection, a two-step masking strategy was implemented. First, water bodies were identified and excluded using NDWI-based thresholding (NDWI > 0) and Otsu's automatic thresholding algorithm (Otsu, 1979).

Second, agricultural areas were masked using the CORINE 2018 Land Cover dataset, thereby minimizing false positives caused by seasonal agricultural activities. The binary outputs were further refined through morphological opening and closing operations (Soille, 2003) to suppress noise and enhance classification smoothness. Burned area severity was subsequently assessed using ΔNBR values, which were stratified into predefined severity classes following established protocols (Miller & Thode, 2007).

For accuracy assessment, a confusion-matrix–based evaluation was conducted in accordance with best practices in remote sensing validation (Congalton & Green, 2019). Stratified random sampling was performed on high-resolution reference imagery, and standard metrics including Overall Accuracy (OA), Producer's Accuracy (PA), User's Accuracy (UA), and the Kappa coefficient were calculated.

3.1 Data Preprocessing

The Sentinel-2 images were first subjected to atmospheric correction using the Sen2Cor processor, thereby converting them into surface reflectance products (Level-2A). To ensure the removal of unwanted pixels such as clouds and cloud shadows, a masking procedure was applied using the Scene Classification Layer (SCL). Furthermore, to guarantee geometric consistency between acquisition dates, post-fire images were co-registered to the corresponding pre-fire scenes, with the registration accuracy visually validated and maintained below a root mean square error (RMS) of 0.5 pixels.

3.2 Spectral Index Calculations

Spectral indices are essential tools widely used in the detection and assessment of post-fire impacts using satellite imagery. These indices are specifically designed to capture changes in land surface properties caused by fire events, enabling the distinction between vegetation, water bodies, and burned areas by exploiting variations in reflectance across different portions of the electromagnetic spectrum. In this study, the Normalized Difference Vegetation Index (NDVI), Normalized Burn Ratio 1 (NBR1), Normalized Burn Ratio 2 (NBR2), and the Normalized Difference Water Index (NDWI) were utilized to assess pre- and post-fire land cover changes. NDVI is a widely adopted vegetation index used to estimate vegetation density and vitality, based on the contrast between red and near-infrared (NIR) reflectance (Tucker, 1979). NDVI effectively captures photosynthetic activity, making it an essential indicator for analyzing vegetation condition before and after wildfire events. The Normalized Burn Ratio (NBR), on the other hand, has become a standard index for mapping fire-affected areas and evaluating fire severity (Key & Benson, 2006). NBR utilizes NIR and short-wave infrared (SWIR) bands, which are particularly responsive to fire-induced changes in vegetation structure and moisture. In burned areas, NIR reflectance typically decreases due to vegetation loss, while SWIR reflectance increases because of exposed soil and ash. This spectral contrast enables effective discrimination of burned regions. In arid and semi-arid ecosystems, where post-fire vegetation recovery is slower, NBR has shown high performance in detecting fire scars (Veraverbeke et al., 2012). Moreover, when used in temporal analyses, NBR offers significant advantages in monitoring post-fire vegetation dynamics and recovery trends (Parks et al., 2014). The Normalized Difference Water Index (NDWI) is employed to identify and monitor water bodies using NIR and SWIR reflectance values (Gao, 1996; McFeeters, 1996). NDWI enhances the visibility of water features while suppressing vegetation and soil signals, making it particularly useful for isolating hydrological features in post-fire landscapes. Additionally, it serves as a valuable indicator for assessing changes in water availability and hydrological conditions after wildfire events. Table 2 provides band assignments for major satellite sensors, enabling researchers to apply the same spectral index calculations regardless of their chosen platform:

Table 2. Sentinel-2 spectral band assignments for index calculations

Spectral Region	*Wavelength (nm)*	*Sentinel-2*
Red	640-680	B4 (665)
NIR	840-880	B8 (842)
NIR-narrow	860-870	B8A (865)
SWIR1	1550-1750	B11 (1610)
SWIR2	2100-2300	B12 (2190)

In this study, spectral indices were calculated using the Sentinel-2 images. The specific band designations used were: Red = B4 (665 nm), NIR = B8 (842 nm), NIR-narrow = B8A (865 nm), SWIR1 = B11 (1610 nm), and SWIR2 = B12 (2190 nm). These indices were calculated for both pre-fire and post-fire Sentinel-2 images using Equations 1 – 4. While NDVI

was preferred for monitoring pre-fire vegetation cover, NBR1 and NBR2 were used in the analysis of post-fire vegetation changes. On the other hand, NDWI was employed as an effective tool in post-fire detection of water bodies.

$$\mathrm{NDVI} = \frac{(\mathrm{B8} - \mathrm{B4})}{(\mathrm{B8} + \mathrm{B4})} \quad (1)$$

$$\mathrm{NBR1} = \frac{(\mathrm{B8} - \mathrm{B12})}{(\mathrm{B8} + \mathrm{B12})} \quad (2)$$

$$\mathrm{NBR2} = \frac{(\mathrm{B11} - \mathrm{B12})}{(\mathrm{B11} + \mathrm{B12})} \quad (3)$$

$$\mathrm{NDWI} = \frac{(\mathrm{B3} - \mathrm{B8})}{(\mathrm{B3} + \mathrm{B8})} \quad (4)$$

Delta Normalized Difference Vegetation Index (ΔNDVI) and Delta Normalized Burn Ratio (ΔNBR) are measures that express the difference in spectral index values obtained at different times. They are used particularly to evaluate the effects of events such as fire on ecosystems. ΔNBR expresses the difference between NBR values obtained before and after fire. This index provides information about the severity and damage of the fire. ΔNDVI expresses the difference between NDVI values obtained before and after fire and is used to evaluate changes in vegetation cover (Tucker, 1979). These spectral indices were calculated using Equations 5 – 7, where NDVI_t1 and NDVI_t2 respectively represent the NDVI values calculated from images collected at t1 and t2 dates. Similarly, NBRt1 and NBRt2 represent the NBR values computed at t1 and t2 dates, while NBR2t1 and NBR2t2 represent the NBR2 values at times t1 and t2. Δ-indices (Equations 5–7) were calculated as the difference between pre-fire and post-fire values, providing temporal change metrics particularly useful for assessing burn severity and vegetation loss:

$$\Delta NDVI = NDVIt_2 - NDVIt_1 \quad (5)$$

$$\Delta\mathrm{NBR1} = \mathrm{NBR1t_2} - \mathrm{NBR1t_1} \quad (6)$$

$$\Delta NBR2 = NBR2t_2 - NBR2t_1 \quad (7)$$

3.3 Burn Area Detection

The methodology involved a systematic processing chain applied to difference indices (ΔNDVI, ΔNBR1, and ΔNBR2) calculated from pre- and post-fire satellite images. Initially, a water mask was generated using the Normalized Difference Water Index (NDWI > 0) threshold and applied to exclude water surfaces from all three difference indices, with water-covered pixels set to "NoData" values to ensure fire impact assessments focused exclusively on terrestrial vegetation areas. The SCL-based masking was applied to eliminate atmospheric artifacts and cloud shadows, while the NDWI thresholding step specifically targeted residual inland water surfaces undetected by the SCL layer. This two-step approach ensured complete removal of non-vegetated reflectance anomalies. Following water masking, each difference index was independently classified into burned and unburned areas using the Otsu Automatic Thresholding algorithm (Otsu, 1979), which was applied globally to the entire study area histogram for each index without class-specific parameter tuning. Otsu thresholds were computed from the global histogram of ΔNDVI, ΔNBR1, and ΔNBR2 images, yielding optimal cut-off values of −0.18, −0.23, and −0.25, respectively. These values were empirically validated to separate burned and unburned pixel clusters. Otsu thresholding was selected over manual thresholding to ensure reproducibility and eliminate subjective bias. The algorithm determines optimal threshold by minimizing within-class variance across the entire image histogram. This binary classification approach effectively separated burned areas (showing significant vegetation loss) from unburned areas (showing minimal or no vegetation change). Subsequently, morphological operations were applied to improve spatial coherence of the classification results, including opening operations (disk radius = 1 pixel) to remove isolated single-pixel noise and closing operations (disk radius = 2 pixels) to merge adjacent burn patches and fill small gaps within burned areas Morphological operations employed a disk-shaped structuring element with radius of 1 pixel for opening (noise removal) and 2 pixels for closing (gap filling), following standard practices in binary image processing (Soille, 2003). In the resulting classification maps, black areas represent masked water surfaces, light gray areas indicate burned areas with significant vegetation change, and dark gray areas represent unburned areas with minimal vegetation change. This systematic approach eliminates water surface interference in fire impact assessments, provides accurate burned area delineation over terrestrial surfaces, and

supports effective post-fire rehabilitation and planning studies by ensuring reliable burn severity mapping for each spectral index.

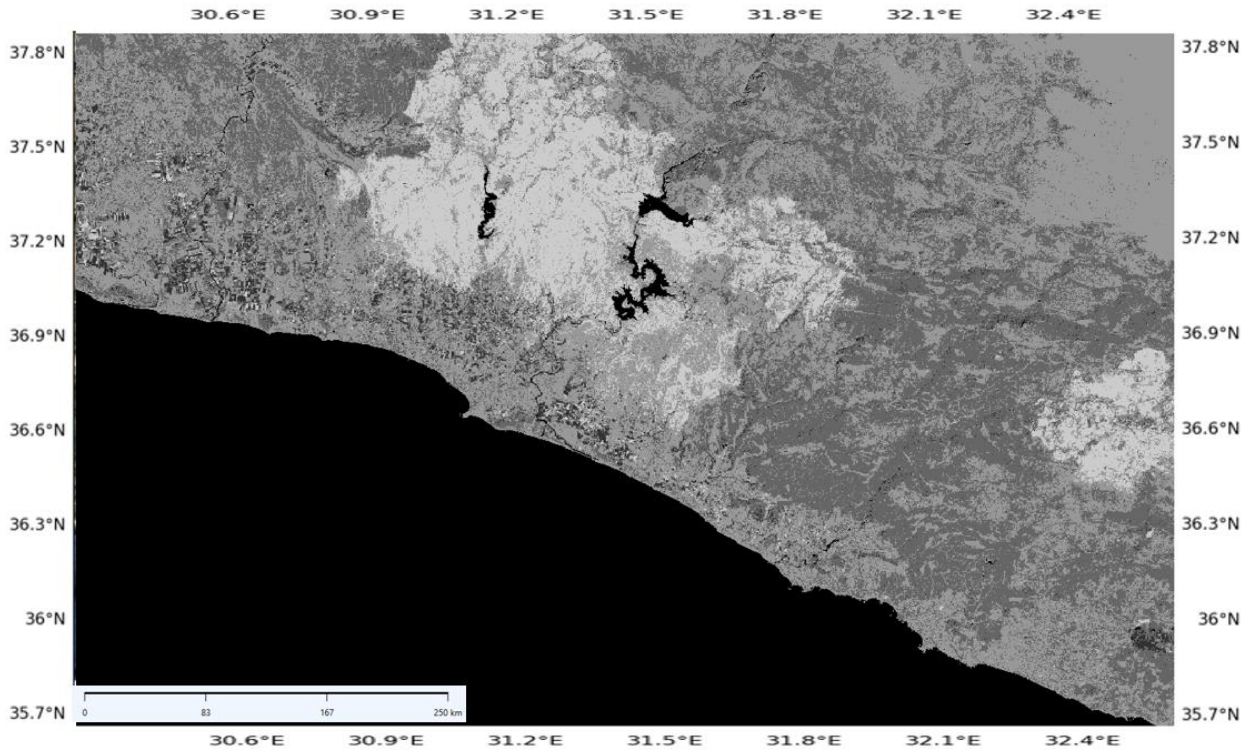

Figure 4. NDVI after Otsu thresholding

The image difference method for detecting burned areas faces a significant challenge from agricultural lands, which exhibit spectral changes between pre- and post-fire dates due to harvest seasons rather than fire damage. These harvest-induced reflectance variations can mimic fire-related spectral signatures, leading to false positives in burned area classification. To address this limitation, agricultural areas were systematically excluded from the Otsu-classified results using the CORINE Land Cover 2018 dataset. The masking process involved rasterizing specific CORINE classes at 10-meter resolution and applying an AND-NOT operation to remove agricultural pixels from the binary burned area maps derived from ΔNDVI, ΔNBR1, and ΔNBR2. Although CORINE data have coarser spatial resolution (100 m), vector-based rasterization and majority resampling were applied to align with 10 m Sentinel-2 grids. This ensured accurate overlay and minimized edge misalignment during the masking process. CORINE polygons were rasterized to a 10 m grid using majority resampling (pixel assigned to the CORINE class covering the largest fraction of the pixel). Edge pixels with mixed classes were assigned based on >50% area rule; these operations minimize systematic bias when applying the agricultural mask to Sentinel-2 data. The agricultural mask comprised CORINE Level-2 and Level-3 classes including arable land (non-irrigated and irrigated), permanent crops (vineyards, fruit trees, olive groves), pastures, and heterogeneous agricultural areas (complex cultivation patterns, land principally occupied by agriculture with significant natural vegetation, and agro-forestry areas). Additionally, CORINE Level-1 "Artificial surfaces" were excluded to focus the analysis on natural vegetation areas. This targeted masking approach effectively minimized harvest-related misclassifications while preserving the detection of actual fire-induced vegetation changes in natural and semi-natural terrestrial environments. Figure 5 demonstrates the spatial distribution of these masked agricultural regions within the study area, displayed in black, showing their prevalence particularly in cultivated valleys and plateaus where seasonal crop cycles could otherwise interfere with accurate burn severity assessment.

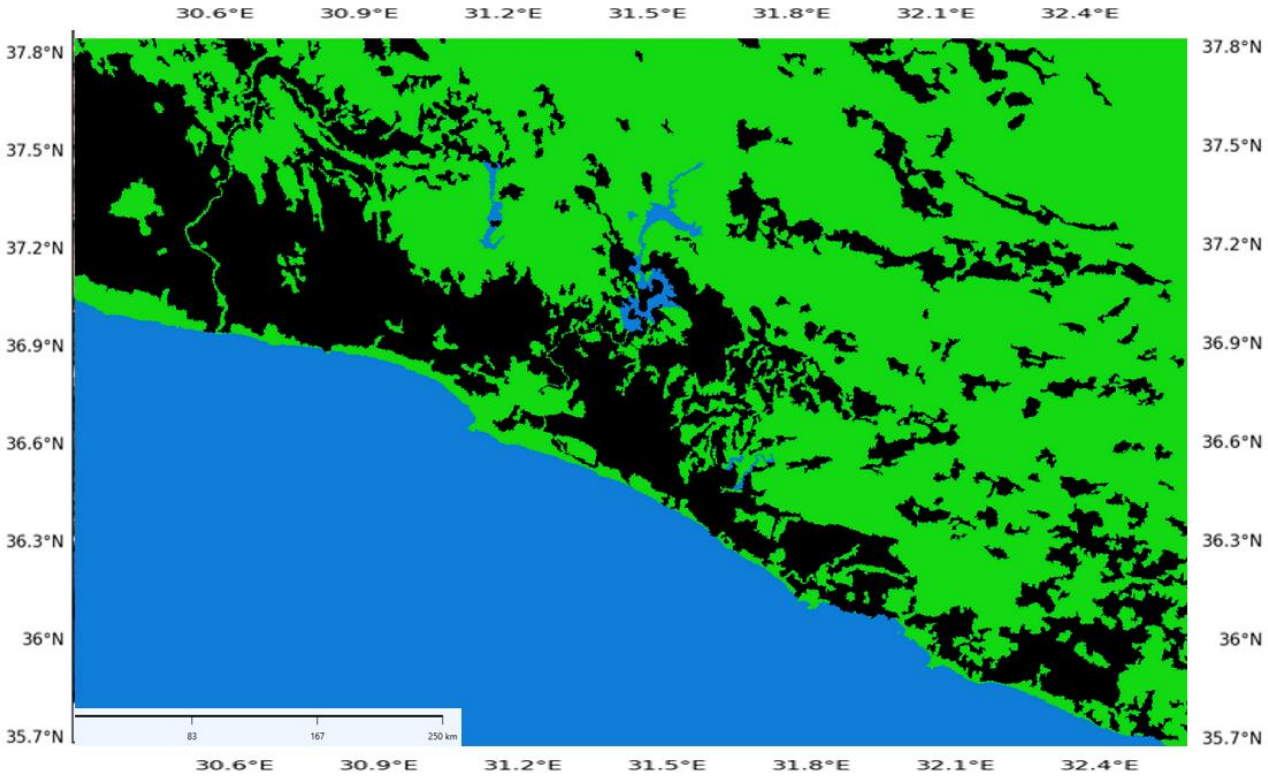

Figure 5. Burned area classification result from ΔNDVI index after agricultural area masking, showing the spatial distribution of CORINE 2018-derived agricultural mask (black areas) within the study area

3.4 Burn Severity Analysis

Burn severity analysis is a method used to determine the intensity and extent of forest fires (Key & Benson, 2006). This analysis is conducted through the examination of post-fire changes on satellite images. Burn severity maps provide important information for planning post-fire rehabilitation studies by visualizing the effects of fire on the ecosystem. Burn severity is generally calculated based on changes in the NBR index. In this study, pre- and post-fire burn severity was calculated based on changes in the NBR index. In this context, ΔNBR was calculated using pre- and post-fire NBR values, and burn severity classes were created according to determined threshold values (Miller & Thode, 2007). The calculated ΔNBR values were classified from high to low, and changes that occurred in the post-fire ecosystem were analyzed. It should be noted that the ΔNBR severity thresholds employed in this study were originally developed in U.S.-based ecosystems (Key & Benson, 2006; Miller & Thode, 2007). These thresholds have been widely adopted in the remote sensing literature, yet they may not directly be transferred to Mediterranean landscapes such as Turkey, where vegetation structure, soil background, and fire regimes differ substantially. Consequently, the severity class estimates presented here should be interpreted with caution. Although ΔNBR thresholds were derived from U.S. ecosystems, this limitation also highlights an opportunity to develop region-specific thresholds for Mediterranean regions such as Türkiye, where vegetation composition and soil background differ significantly. Future studies should focus on data-driven approaches, such as histogram natural breaks, k-means clustering, or Jenks optimization in order to enhance the ecological validity of burn severity assessments in Mediterranean ecosystems.

3.5 Accuracy Assessment

Confusion matrices were constructed to calculate comprehensive accuracy metrics for the burned area classifications. From these matrices, Overall Accuracy (OA), Producer's Accuracy (PA), User's Accuracy (UA), and Kappa Coefficient values were derived following established protocols (Congalton, 1991). OA represents the ratio of correctly classified samples to the total number of samples, indicating the overall classification success. PA shows the proportion of reference samples belonging to a class that are correctly classified, demonstrating how well each class is detected by the algorithm (Foody, 2002). UA represents the proportion of classified samples that actually belong to their assigned class, indicating the reliability and commission error rate of the classification results (Story & Congalton, 1986).

The Kappa Coefficient measures classification performance relative to random chance, calculated using the confusion matrix diagonal values, marginal totals, and overall sample size (Cohen, 1960). Stratified random sampling was employed to ensure balanced representation across burned and unburned classes, addressing potential class imbalance issues that could bias accuracy assessment results (Stehman, 2009). This approach guarantees equal sample allocation to each class regardless of their spatial extent, providing robust statistical evaluation particularly important when rare classes might be underrepresented in purely random sampling schemes. The reference dataset was created through visual interpretation of very high-resolution Google Earth imagery (1-meter spatial resolution) acquired during the post-fire period (September-December 2021). This interpretation process was enhanced using Google Earth's embedded time-slider functionality, allowing analysts to examine temporal changes and confirm fire-related vegetation loss by comparing pre- and post-fire conditions. Each reference sample corresponded to a 20×20 m window, consistent with Sentinel-2's SWIR band resolution, to ensure spatial homogeneity. Samples were binary classified as either burned or unburned, with ambiguous boundary cases excluded to maintain labeling consistency and reduce interpretation uncertainty. Validation samples were distributed using stratified random sampling across burned and unburned classes within natural and semi-natural land covers. Agricultural pixels identified by CORINE were excluded from both classification and validation samples to prevent harvest-related spectral changes from biasing the confusion matrices. In other words, CORINE masking was applied prior to sample selection to ensure validation reflects detection performance over target (vegetated) surfaces only. A total of 2,400 validation samples were distributed across the study area using stratified random sampling, with equal allocation of 1,200 samples to each class (burned and unburned). Since no explicit training phase was required for the Otsu thresholding approach, all collected samples served validation purposes exclusively. Accuracy metrics including OA, UA, PA, and Kappa coefficient were calculated from the resulting confusion matrices, with 95% confidence intervals estimated using the binomial distribution approach to quantify statistical uncertainty. Numerically, the 95% confidence intervals for Overall Accuracy (binomial approximation) are: NDVI = 97.1% ± 0.95 percentage points, NBR1 = 96.3% ± 1.07 percentage points, and NBR2 = 96.8% ± 1.00 percentage points. The spatial distribution of validation samples in relation to the classified ΔNDVI values is illustrated in Figure 6, demonstrating the representative coverage achieved across the spectral range of fire-affected areas.

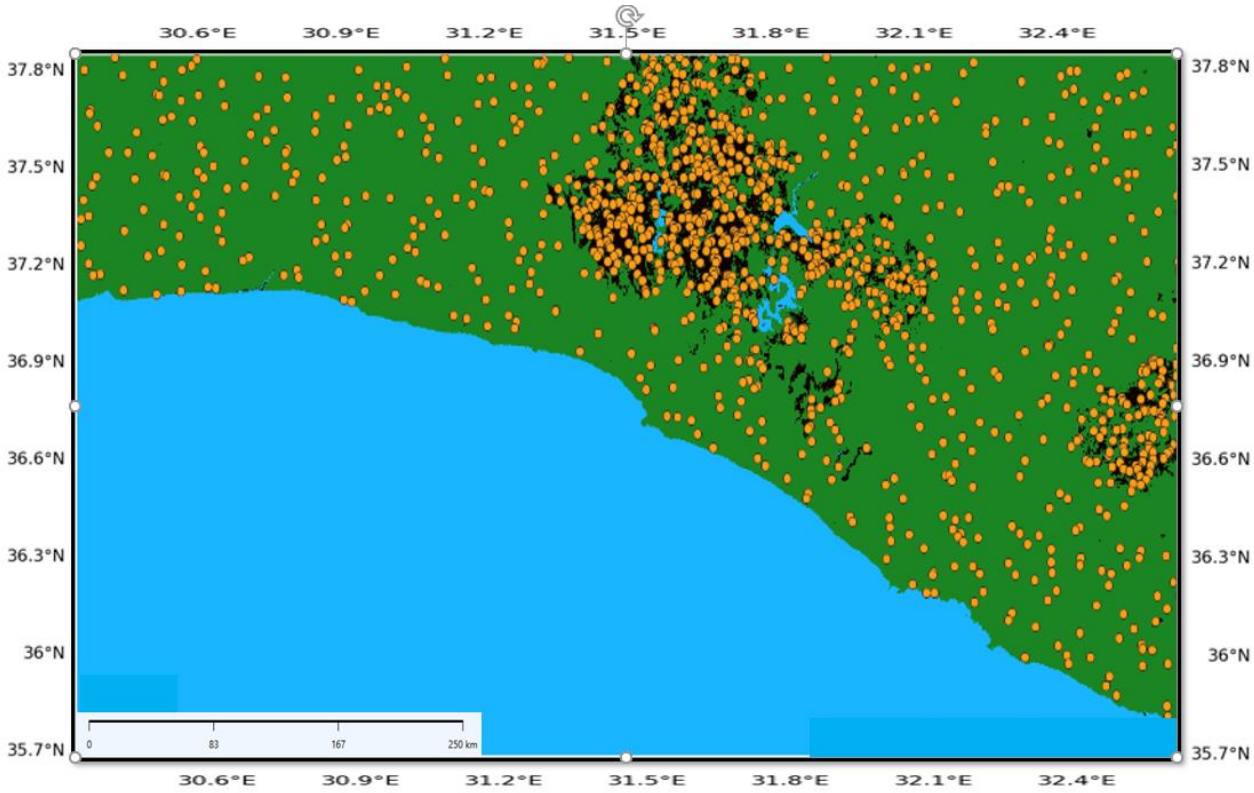

Figure 6. Spatial distribution of stratified random validation samples (1,200 burned and 1,200 unburned) overlaid on the ΔNDVI difference image, demonstrating representative sampling coverage across fire-affected and unaffected areas within the study region.

4. Result and Discussion

4.1 Spectral Indices Analysis of Pre- and Post-Fire Sentinel-2 Data

Each methodological step was designed to ensure logical consistency between spectral preprocessing, index computation, masking, and validation. The NDVI, NBR1, and NBR2 indices derived from pre- and post-fire Sentinel-2 imagery are shown in Figures 7 and 8. Pre-fire NDVI values ranged from -0.2 to 0.8, decreasing to -0.4 to 0.3 after the fire, clearly reflecting substantial vegetation loss in burned areas. In some locations, NDVI reached negative values, which corresponds to a near-complete removal of green biomass. As NDVI approaches -1, vegetation cover diminishes, whereas values closer to +1 indicate healthier and denser vegetation. The sharp reductions observed after the event therefore confirm the severity of canopy loss within the burned perimeter.

A similar pattern was observed for the NBR1 index, which showed high values before the fire and a pronounced decline afterward, consistent with the reduction of healthy vegetation cover (Coppin et al., 2004). The NBR2 index exhibited comparable pre- to post-fire decreases, supporting its utility as an effective indicator for burned area identification (Tiengo et al., 2025). In addition, NDWI was analyzed to assess changes in surface moisture conditions. Although not primarily developed for burn severity assessment, NDWI values also decreased after the fire, likely due to the loss of moisture from both vegetation and upper soil layers. NDWI was examined only for the pre-fire period, as the fire did not affect any major water bodies; thus, post-fire NDWI analysis was considered unnecessary for this study.

Recent studies provide additional context for interpreting these spectral changes. Arikan and Yildiz (2023) demonstrated that extensive forest fires in Antalya were closely associated with subsequent air quality deterioration, as detected through satellite-based monitoring on the Google Earth Engine platform. Our findings complement theirs by quantifying both the spatial extent and severity of burned areas, information that can serve as a direct input for atmospheric dispersion modeling. Notably, the zones we identified as high severity overlap with areas of elevated particulate matter reported by Arikan and Yildiz, suggesting strong potential for integrating burned area severity maps into post-fire air quality and health impact assessments.

Similarly, Makineci (2024) emphasized the advantages of combining optical, SAR, and very high-resolution commercial imagery to map burned areas during the Rhodes 2023 fires. While our study relies primarily on Sentinel-2 spectral indices supported by CORINE land-cover masking, the high overall accuracies achieved indicate that such an approach can be operationally effective in Mediterranean forest–agriculture mosaics. Nevertheless, as highlighted by Makineci, incorporating SAR or high-resolution imagery could further reduce omission and commission errors, particularly in complex terrain or wildland–urban interface (WUI) zones.

Finally, Alkan and Karasaka (2024) demonstrated the capability of U-Net-based deep learning models for burned area segmentation, with particularly strong results when high-quality training data were available. Although our index-based approach achieves comparable accuracy (OA ≈ 97%) without requiring annotated datasets, the comparison underscores an important trade-off: supervised deep learning offers higher adaptability at the cost of data requirements and computational complexity, whereas index differencing is rapid, reproducible, and suitable for operational workflows. A promising direction for future research is a hybrid pipeline in which spectral index differencing provides an initial mask that is subsequently refined using U-Net or similar architectures, combining the strengths of both approaches.

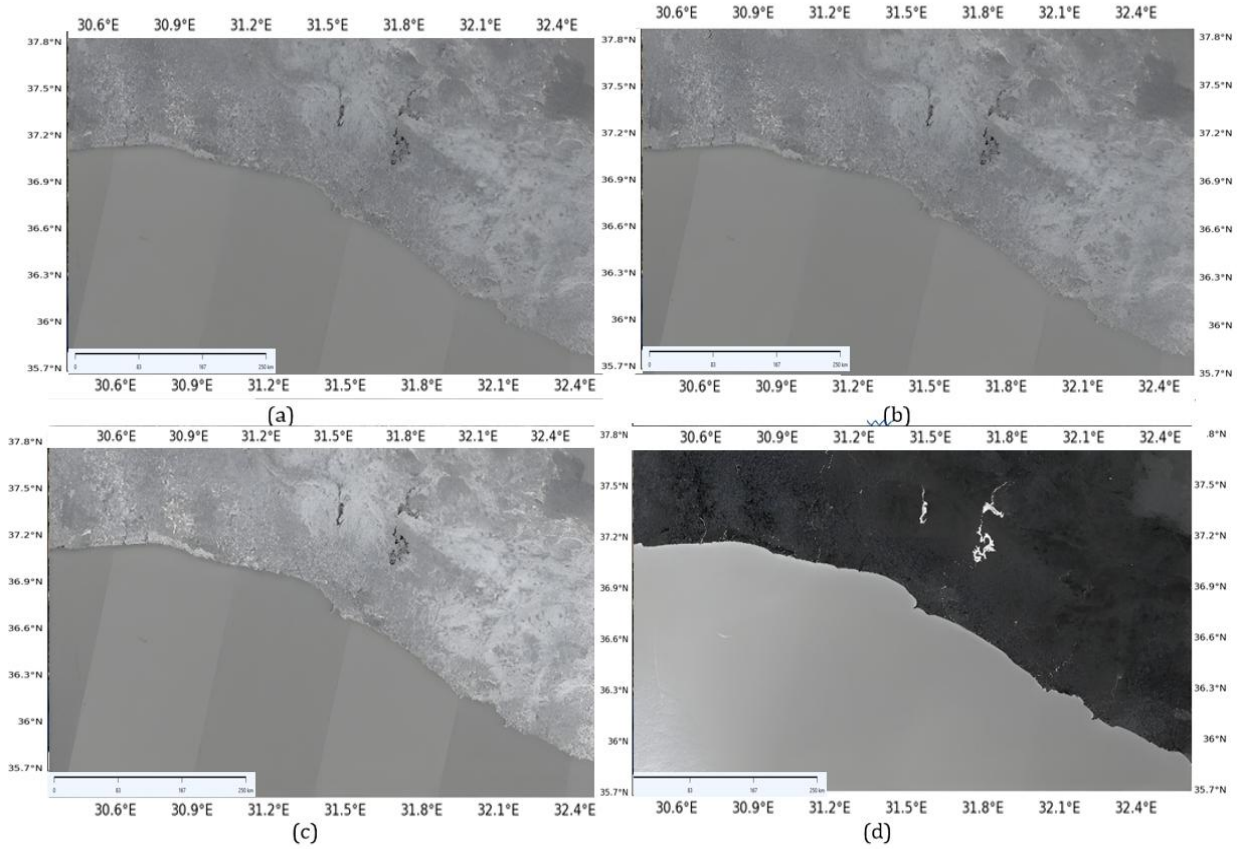

Figure 7. Spectral indexes computed for pre-fire image: a) NDVI, b) NBR1, c) NBR2, d) NDWI

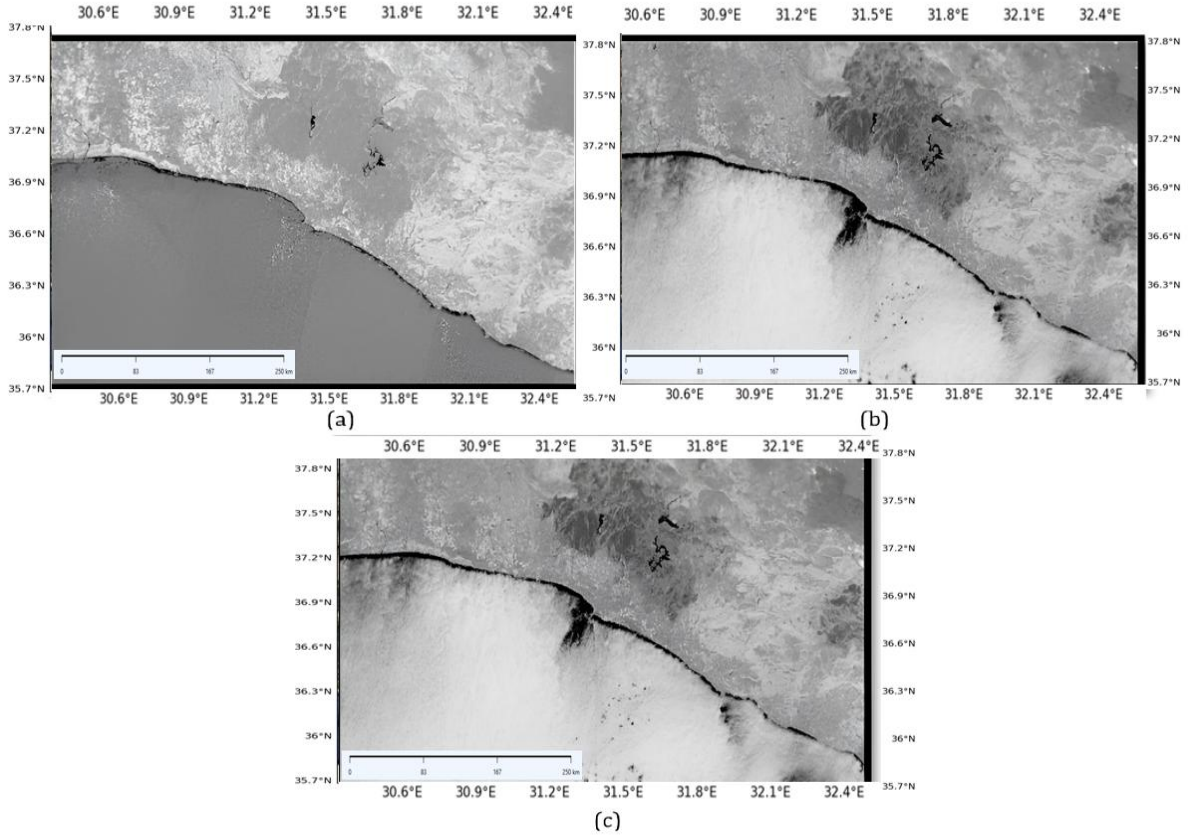

Figure 8. Spectral indexes computed for post-fire image: a) NDVI, b) NBR1, c) NBR2

4.2 The Results of Difference Spectral Indices and Accuracy Assessment

The computed difference spectral indices (ΔNDVI, ΔNBR1, and ΔNBR2) are presented in Figure 9, illustrating the spectral changes between pre- and post-fire conditions across the study area. These indices effectively capture vegetation loss and structural alterations in canopy and soil properties caused by fire, with high difference values corresponding to areas experiencing the most severe fire impacts. ΔNDVI primarily reflects changes in photosynthetically active vegetation, while ΔNBR1 and ΔNBR2 provide enhanced sensitivity for detecting burned surfaces through their incorporation of shortwave infrared reflectance, which is particularly responsive to fire-induced changes in vegetation structure and soil exposure. Figure 10 demonstrates the application of the CORINE 2018-based agricultural land mask to the difference index results, showing how agricultural areas (displayed in designated colors) are systematically excluded from burned area classification to prevent harvest-induced spectral changes from being misinterpreted as fire damage. This masking process is essential for reducing false positives in agricultural regions where seasonal crop cycles can produce spectral signatures similar to those caused by fire. The comparison between masked and unmasked results clearly illustrates the importance of agricultural area exclusion in improving classification accuracy, particularly in mixed agricultural-natural landscapes where temporal spectral changes from multiple sources can confound burned area detection. The integration of ΔNDVI, ΔNBR1, and ΔNBR2 with appropriate masking procedures provides a robust framework for assessing fire severity and extent while minimizing classification errors from non-fire related spectral changes.

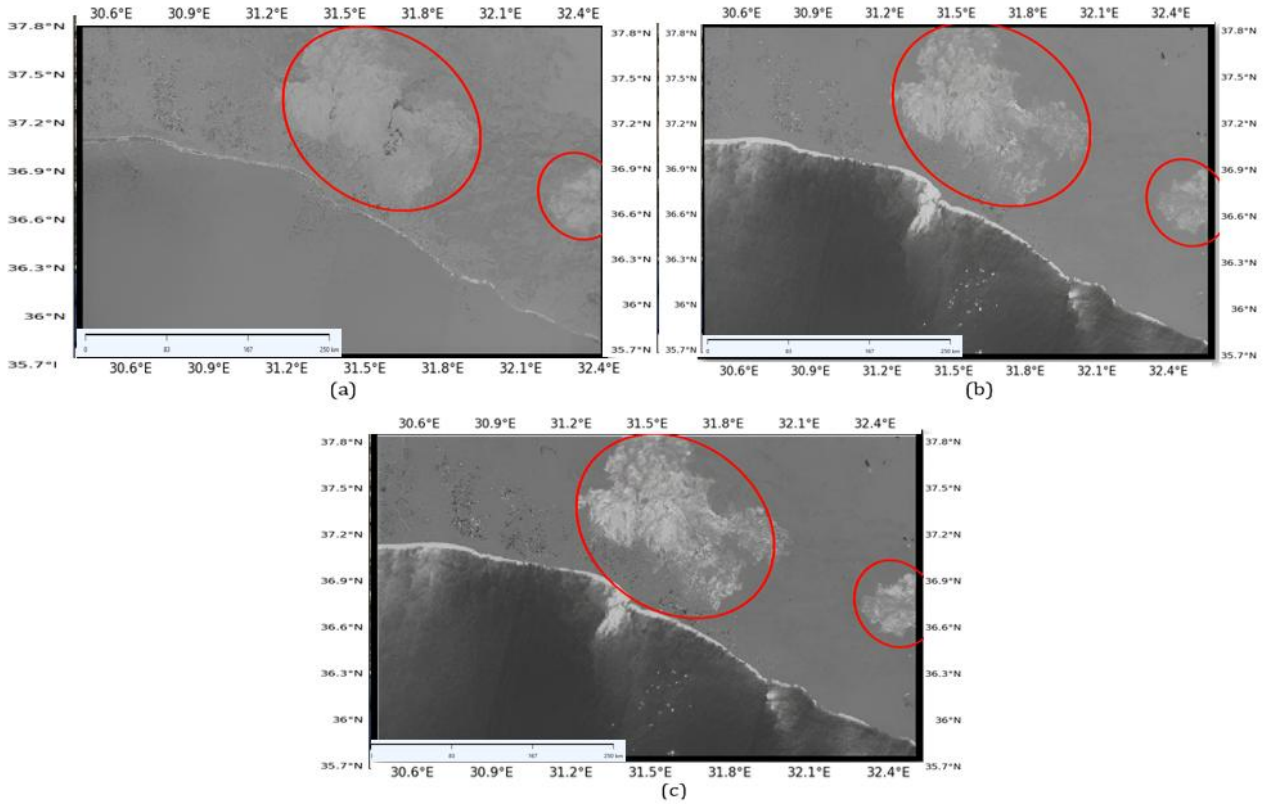

Figure 9. Difference spectral indexes: a) ΔNDVI, b) ΔNBR1, c) ΔNBR2

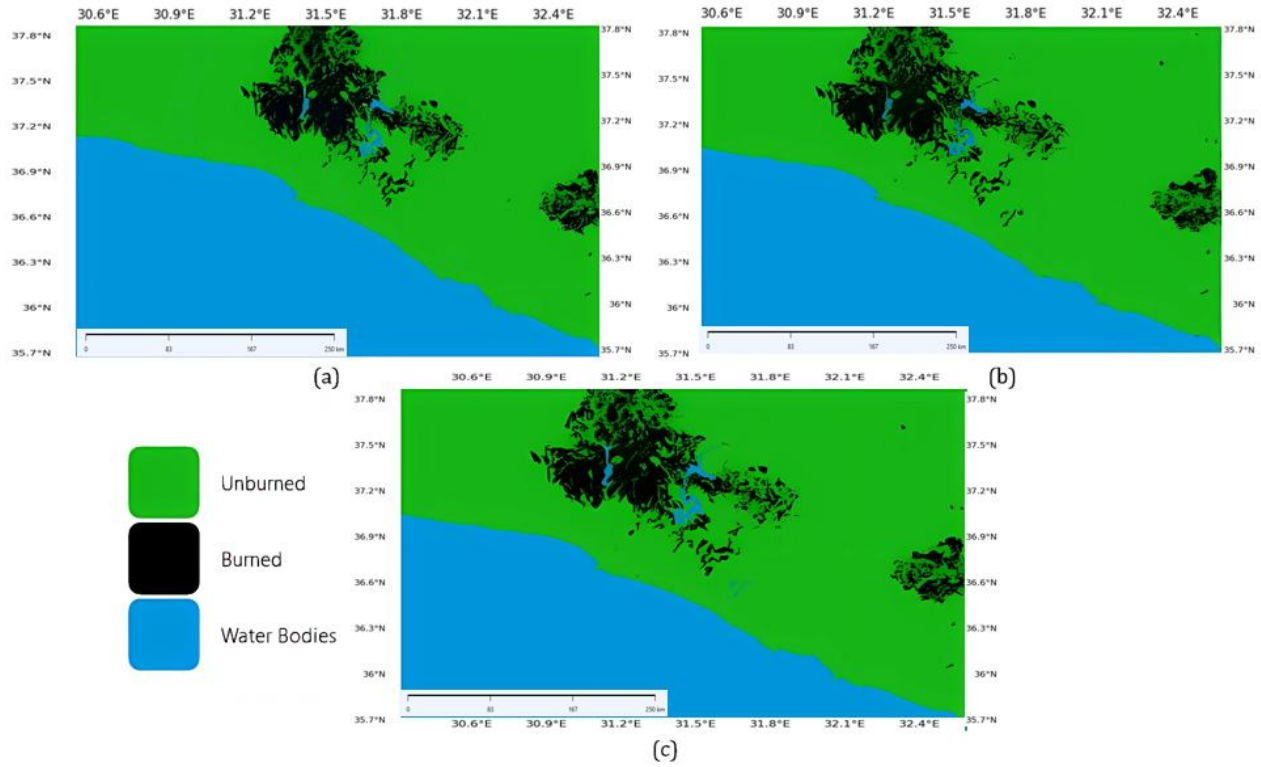

Figure 10. Comparison of Otsu thresholding results before and after CORINE 2018 agricultural mask application for a) ΔNDVI, b) ΔNBR1, and c) ΔNBR2 indices, showing the exclusion of agricultural areas (masked regions) to prevent harvest-related misclassification as burned areas

The confusion matrix calculated from NDVI-based detection results is presented in Table 3. As seen in the table, for burned areas, 580 out of 600 total samples were correctly detected, corresponding to a UA value of 95.0%. For unburned areas, 587 out of 600 samples were correctly identified, yielding a UA of 97.8%. The obtained OA was 97.1%, demonstrating a highly accurate classification performance. Additionally, the calculated Kappa coefficient (KP) of 0.950 confirms that the classification results are well beyond random agreement and reflect strong consistency. For the burned area class, the PA was calculated as 98.0%, while the UA was 95.0%. For the unburned area class, PA and UA values were 96.7% and 97.8%, respectively. These results clearly demonstrate that the NDVI-based detection approach provided highly accurate and reliable performance in distinguishing between burned and unburned areas.

Table 3: Error matrix computed from the results of NDVI based burnt area detection

Class	C1	C2	TOTAL	UA (%)	PA (%)
C1	580	20	600	95.0	98.0
C2	13	587	600	97.0	97.0
TOTAL	593	607	1200	-	-
UA (%)	95.0	97.8	-	97.1	-
PA (%)	98.0	96.7	-	-	97.1

OA: 97,1%, KP: 0.950

KP: Kappa, OA: Overall Accuracy, C1: Burned Area, C2: Unburned Area, TOTAL: Total, UA: User Accuracy, PA: Producer Accuracy

The confusion matrix computed based on the results of NBR1-based burned area detection is presented in Table 4. The OA obtained from this index was 96.3%, and the Kappa coefficient (KP) was computed as 0.950. For the burned area class (C1), PA was computed as 97.0%, and UA was computed as 95.0%. For the unburned area class (C2), PA and UA values were calculated as 96.0% and 97.0%, respectively. These results demonstrate that the NBR1-based approach also provided highly accurate and reliable performance in detecting burned areas.

Table 4: Error matrix computed from the results of NBR1 based burnt area detection

Class	C1	C2	TOTAL	UA (%)	PA (%)
C1	574	26	600	95.0	97.0
C2	20	580	600	97.0	95.7
TOTAL	592	606	1200	-	-
UA (%)	95.0	97.0	-	96.3	-
PA (%)	97.0	95.7	-	-	97.0

OA: 96.3%, KP: 0.950

The confusion matrix computed based on the results of NBR2-based burned area detection is presented in Table 5. The OA obtained from this index was 96.8%, and the Kappa coefficient (KP) was computed as 0.940. For the burned area class (C1), PA was computed as 96.2%, and UA was computed as 97.0%. For the unburned area class (C2), PA and UA values were calculated as 97.3% and 96.2%, respectively. These results demonstrate that the NBR2-based approach also provided highly accurate and reliable performance in distinguishing burned from unburned areas.

Table 5: Error matrix computed from the results of NBR2 based burnt area detection

Class	C1	C2	TOTAL	UA (%)	PA (%)
C1	584	16	600	97.0	96.2
C2	23	577	600	96.2	97.3
TOTAL	607	593	1200	-	-
UA (%)	97.0	96.2	-	96.2	-
PA (%)	96.2	97.3	-	-	97.3

OA: 96.8%, KP: 0.940

4.3 Burn Severity Distribution and Performance Comparison

Table 6 shows the spatial distribution of post-fire burn severity classes in the region. According to analysis results, about 1,604.02 hectares of high-severity burned area constitute 1.99% of the total area. These areas represent the regions showing the most severe impact of the fire. Moderate-high severity burned areas cover about 1,867.42 hectares, comprising 2.31% of the total burned area. This burn severity class represents regions where the fire's impact has decreased but still shows significant damage. Moderate-low severity burned areas, calculated as 2,576 hectares, constitute 3.19% of the total burned areas. In these regions, the fire's impact is relatively more limited. Low-severity burned areas cover 5.16% of the total burned areas, spreading over an area of 4,160.72 hectares. In this class, although the fire's impact is low, there is still a certain level of damage.

Enhanced regrowth areas represent regions where vegetation has regenerated itself after the fire. Low-severity regrowth constitutes 2.71% (2,190.28 ha) of the total area, while high-severity regrowth comprises 1.21% (974.75 ha). The unburned class includes regions unaffected by the fire and covers 67,320.64 hectares, equivalent to 83.43% of the total area. The burn severity analysis results are shown in Figure 11.

Table 6. Spatial distribution of burn severity classes

BURN SEVERITY CLASS	Area (hectares)	Percentage of Total Area
High Severity	1604.02	1.99
Moderate-High Severity	1867.42	2.31
Moderate-Low Severity	2576.00	3.19
Low Severity	4160.72	5.16
Low Regrowth	2190.28	2.71
High Regrowth	974.75	1.21
Unburned	67320.64	83.43

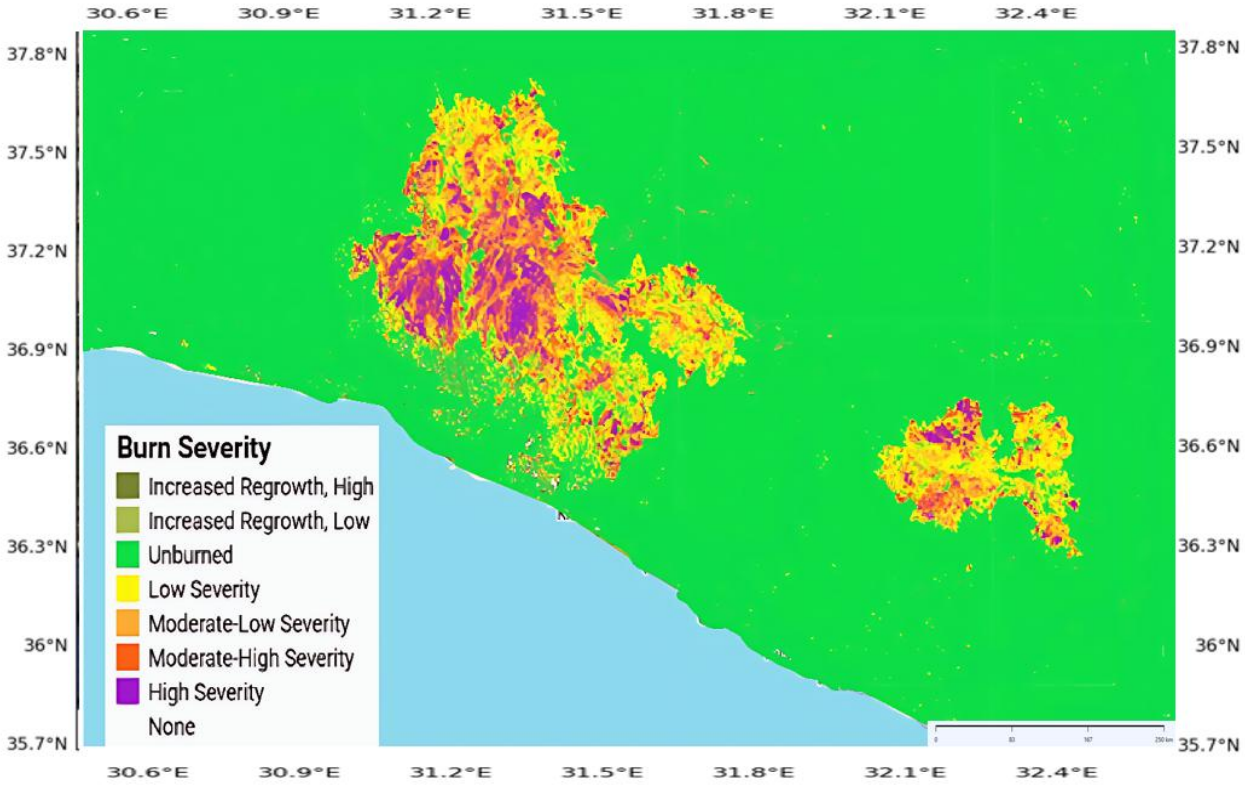

Figure 11. The results of burn severity analysis

4.4 Performance Comparison of Spectral Indices and Visual Assessment

To evaluate the effectiveness of different spectral indices in burned area detection, a comparative performance analysis was conducted using key accuracy metrics, including UA, PA, Kappa Coefficient, and OA. The results of this analysis are presented in Table 7. Figure 12 shows the burned area detection results based on the NDVI, NBR1 and NBR2 indices. In the figure, the orange circles highlight the areas where changes in the respective indices are significant. Highlighted ellipses indicate areas of spectral discrepancy between indices, particularly over mixed vegetation–soil mosaics. Additionally, F1-score, recall, and precision were computed to provide complementary evaluation metrics for burned area detection performance (Sokolova & Lapalme, 2009).

Table 7. Accuracy assessment of burned area classification based on different spectral indices

Spectral Index	Burned Area User's Accuracy (%)	Burned Area Producer's Accuracy (%)	Kappa Coefficient	Overall Accuracy (%)	Precision (%)	Recall (%)	F1-score (%)
NDVI	95.0	98.0	0.950	97.1	95.0	98.0	96.5
NBR1	95.0	97.0	0.950	96.3	95.0	97.0	96.0
NBR2	97.0	96.2	0.940	96.8	97.0	96.2	96.6

Complementary metrics were computed: NDVI yielded Precision = 95.0%, Recall = 98.0%, and F1-score = 96.5%; NBR1 yielded Precision = 95.0%, Recall = 97.0%, and F1-score = 96.0%; NBR2 yielded Precision = 97.0%, Recall = 96.2%, and F1-score = 96.6%.

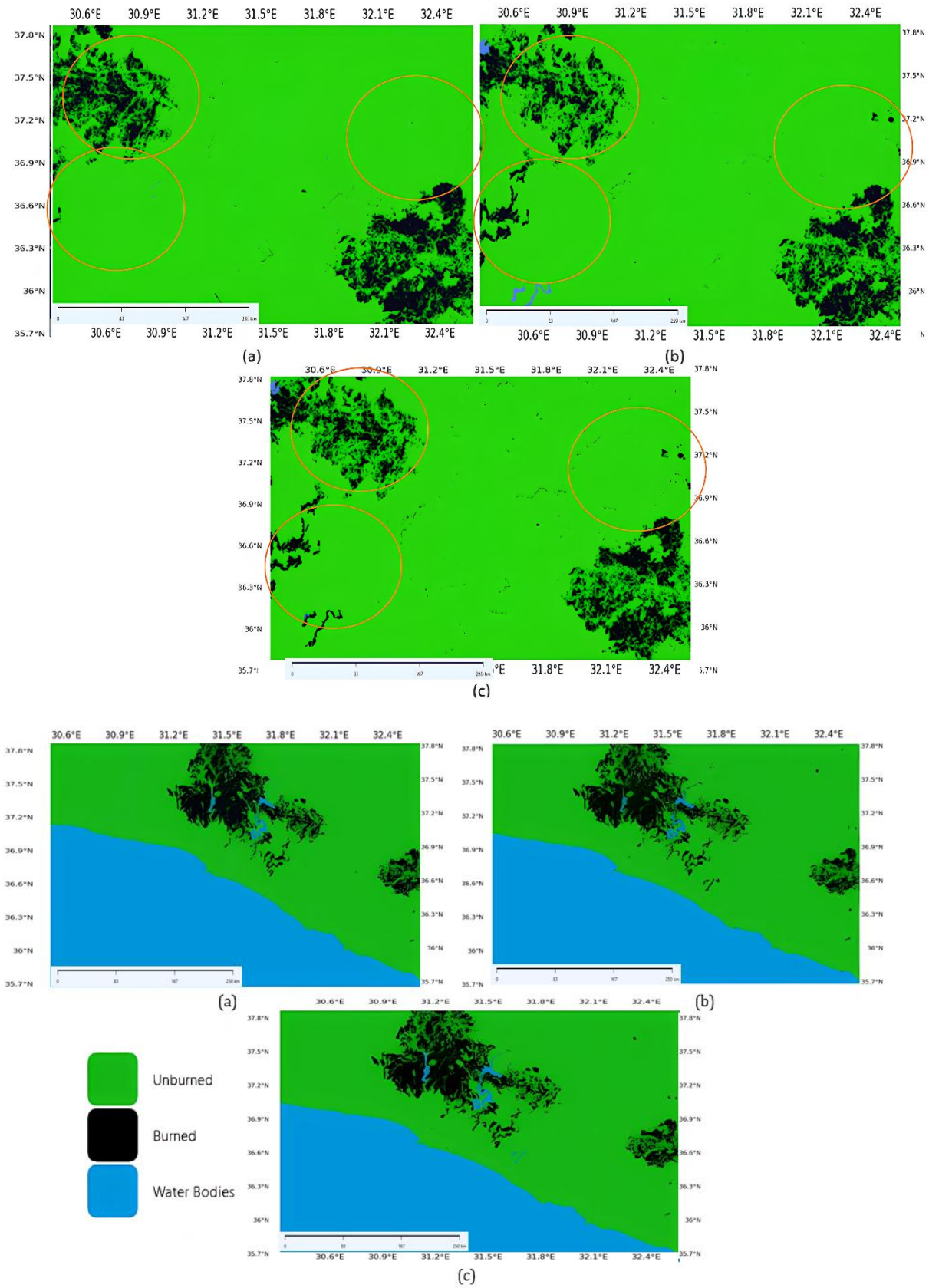

Figure 12. Visual comparison of burned area detection results: (a) NDVI-based classification; (b) NBR1-based classification; (c) NBR2-based classification. Highlighted ellipses indicate areas of spectral discrepancy between indices, particularly over mixed vegetation–soil mosaics. All maps in this figure use the same spatial framing and are shown in UTM Zone 36N (EPSG:32636).

The obtained OA and Kappa values approach the upper bound of the typical accuracy range reported in Mediterranean-focused Sentinel-2 studies (e.g., Fernández-García et al., 2022; Wang et al., 2024). Visual inspection confirms that NDVI provides the highest discriminability for burned area identification, offering excellent contrast between burned and unburned surfaces with clear, well-defined boundaries. For instance, the mean pre-fire NDVI in burned zones decreased from 0.68 ± 0.05 to 0.12 ± 0.04 post-fire, reflecting the combined influence of bare soil exposure and reduced chlorophyll content. This outcome is consistent with the heterogeneous forest–maquis mosaic and substantial fractions of bare soil within the study area, which enhance NDVI's contrast sensitivity. In contrast, NBR1 shows effective performance particularly for high-intensity burned areas, with moderate boundary definition but some confusion in patches where spectral differences with surrounding vegetation are smaller. NBR2 exhibits the lowest distinctness, with limited effectiveness in densely vegetated zones, poorly defined boundaries, and higher integration of burned and unburned surfaces.

These differences can be attributed to the varying sensitivities of the respective spectral band combinations to post-fire reflectance changes. The integration of CORINE 2018 agricultural masks systematically reduced misclassification in croplands, where harvest-driven spectral declines are often confused with fire scars. This masking step substantially lowered the false alarm rate, which is particularly relevant for operational fire monitoring and rapid damage assessment. The severity mapping based on ΔNBR indicates that High and Moderate–High severity classes together account for approximately 4.3% of the burned extent. This relatively limited fraction, combined with the patchy spatial distribution of severity, reflects the influence of topography and prevailing wind regimes on fire behavior. Such heterogeneity is ecologically significant, as it shapes post-fire regeneration dynamics and habitat patterns. Moreover, the occurrence of elevated severity levels within wildland–urban interface (WUI) zones highlight areas where management interventions and mitigation efforts should be prioritized.

While the results achieved in this study align with prior Mediterranean-focused studies in terms of overall accuracy and index performance, a detailed comparison reveals nuanced differences. For instance, Fernández-García et al. (2023) reported slightly lower NDVI discriminability in areas with dense forest cover, whereas this study demonstrates that NDVI remains highly effective even in heterogeneous mosaics, likely due to the substantial bare soil fraction enhancing spectral contrast. The performance patterns of NBR1 and NBR2 are consistent with previous findings; however, the integration of agricultural masking in this study led to a notable reduction in false positives, a factor that has been less emphasized in earlier research. Although NDVI yielded the highest overall accuracy in this case, several studies have demonstrated that dNBR generally provides more stable and ecologically interpretable assessments across a wide range of fire regimes.

From an ecological perspective, the patchy distribution of high-severity areas and their limited spatial extent suggest heterogeneous fire effects, with implications for post-fire vegetation recovery, species recolonization, and habitat connectivity. By explicitly linking spectral index performance, masking strategies, and severity mapping to ecological and operational outcomes, this study provides a more comprehensive interpretation than the prior works. Comparable burned area mapping studies in Mediterranean regions (e.g., Fernández-García et al., 2023; Tiengo et al., 2025) reported overall accuracies between 92–96%, confirming the robustness of our results within expected regional ranges. Ecologically, the limited extent of high-severity burns (1.99%) suggests a mosaic fire pattern typical of Mediterranean ecosystems, where heterogeneity in fuel load and topography drives patchy fire behavior (Keeley, 2009; Pausas et al., 2008). Such spatial variability plays a crucial role in post-fire regeneration, influencing seed dispersal, soil nutrient recovery, and habitat heterogeneity across the landscape. This study has several limitations that should be considered. First, ΔNBR severity thresholds used here were developed for North American ecosystems and may not fully capture Mediterranean vegetation responses see Methods. Second, CORINE 2018 has a nominal resolution of 100 m and may introduce mixed-pixel inaccuracies when resampled to 10 m; although majority resampling was used, some edge effects may remain. Third, field-based validation data were derived from visual interpretation of very high-resolution imagery rather than extensive in-situ plots; future studies should include ground measurements to improve severity calibration. Despite these limitations, the comparative accuracy results provide useful guidance for operational burned area mapping in Turkey.

5. Conclusions

This analysis of the 2021 Manavgat wildfire demonstrates the effectiveness of bi-temporal Sentinel-2 imagery for operational burned area mapping in Mediterranean ecosystems. NDVI-based detection achieved the highest accuracy (97.1% overall accuracy, κ=0.950), followed closely by NBR2 (96.8%) and NBR1 (96.3%). Although NBR2 and NBR1 produced accuracy values close to NDVI, their ability to delineate burned area boundaries was comparatively weaker under conditions of dense vegetation cover and heterogeneous soil backgrounds. The integration of CORINE 2018 land cover data significantly enhanced detection reliability by reducing false positives, particularly in agricultural areas where harvest-related spectral changes frequently mimic fire-induced reflectance patterns.

This highlights the necessity of incorporating ancillary land cover information when monitoring fire-affected Mediterranean agro-forest landscapes. In addition, ΔNBR-based burn severity mapping enabled the identification of different severity levels across the fire perimeter, offering valuable insights for prioritizing ecological restoration, rehabilitation, and forest management strategies in post-fire environments. Beyond index selection, the application of cloud and water masking procedures, together with morphological filtering, further reduced noise and improved classification robustness, emphasizing the importance of a complete pre- and post-processing workflow for operational burned area assessments. Collectively, the findings achieved in this work confirm that spectral index-based approaches applied to Sentinel-2 imagery provide an efficient, reproducible, and cost-effective framework for large-scale wildfire monitoring, with substantial implications for supporting decision-making processes in fire management, disaster response, and long-term ecosystem recovery planning. Study limitations include the use of burn severity thresholds developed for North American ecosystems, which may not fully represent Mediterranean fire regimes. Future research should develop region-specific thresholds and incorporate topographic variables to enhance classification accuracy in Turkey's diverse forest ecosystems.

References

Abatzoglou, J. T., & Williams, A. P. (2016). Impact of anthropogenic climate change on wildfire across western US forests. *Proceedings of the National Academy of Sciences, 113*(42), 11770–11775.

Aksoy, E., & Selim, S. (2024). Burned forest area detection in the Manavgat forest fire using NBR and dNBR indices. *Journal of Recent Activities in Architectural Sciences*, *1*(1), 1–11. https://doi.org/10.5281/zenodo.14563064

Alkan, D., & Karasaka, L. (2024). Image segmentation for burned area detection from satellite imagery using the U-Net deep learning model. *Bulletin of Geophysics & Oceanography, 65*(4), 649–674.

Almeida, M., Ribeiro, L. M., Alves, D., Viegas, D. X., Vaz Pinto, V., Marques, R., & San-Miguel-Ayanz, J. (2023). *Analysis of 2021 critical wildfire events in the Mediterranean region*. European Commission Joint Research Centre. https://doi.org/10.2760/562495

Arıkan, D., & Yıldız, F. (2023). Investigation of Antalya forest fire's impact on air quality by satellite images using Google Earth Engine. *Remote Sensing Applications: Society and Environment, 29,* Article 100922. https://doi.org/10.1016/j.rsase.2023.100922

Bannari, A., Morin, D., Bonn, F., & Huete, A. R. (1995). A review of vegetation indices. *Remote Sensing Reviews, 13*(1–2), 95–120. https://doi.org/10.1080/02757259509532298

Chen, D., Pereira, J. M. C., Masiero, A., & Pirotti, F. (2017). Mapping fire regimes in China using MODIS active fire and burned area data. *Applied Geography, 85,* 14–26. https://doi.org/10.1016/j.apgeog.2017.05.013

Chuvieco, E. (2009). *Earth observation of wildland fires in Mediterranean ecosystems*. Springer.

Chuvieco, E., Aguado, I., Salas, J., García, M., Yebra, M., & Oliva, P. (2020). Satellite remote sensing contributions to wildland fire science and management. *Current Forestry Reports, 6,* 81–96. https://doi.org/10.1007/s40725-020-00116-5

Chuvieco, E., Mouillot, F., van der Werf, G. R., San Miguel, J., Tanase, M., Koutsias, N., García, M., Yebra, M., Padilla, M., Gitas, I., Heil, A., Hawbaker, T. J., & Giglio, L. (2019). Historical background and current developments for mapping burned area from satellite Earth observation. *Remote Sensing of Environment, 225,* 45–64. https://doi.org/10.1016/j.rse.2019.02.013

Cohen, J. (1960). A coefficient of agreement for nominal scales. *Educational and Psychological Measurement, 20(1),* 37–46. https://doi.org/10.1177/001316446002000104

Congalton, R. G. (1991). A review of assessing the accuracy of classifications of remotely sensed data. *Remote Sensing of Environment, 37*(1), 35–46. https://doi.org/10.1016/0034-4257(91)90048-B

Congalton, R. G., & Green, K. (2019). *Assessing the accuracy of remotely sensed data: Principles and practices* (3rd ed.). CRC Press.

Coppin, P., Jonckheere, I., Nackaerts, K., Muys, B., & Lambin, E. (2004). Digital change detection methods in ecosystem monitoring: A review. *International Journal of Remote Sensing, 25*(9), 1565–1596. https://doi.org/10.1080/0143116031000101675

Drusch, M., Del Bello, U., Carlier, S., Colin, O., Fernandez, V., Gascon, F., Hoersch, B., Isola, C., Laberinti, P., Martimort, P., Meygret, A., Spoto, F., Sy, O., Marchese, F., & Bargellini, P. (2012). Sentinel-2: ESA's optical high-resolution mission for GMES operational services. *Remote Sensing of Environment, 120,* 25–36. https://doi.org/10.1016/j.rse.2011.11.026

European Space Agency. (2021). *Sentinel-2 documents and publications*. The European Space Agency (ESA). https://www.esa.int/Applications/Observing_the_Earth/Copernicus/Sentinel-2/Sentinel-2_documents_and_publications

Fernández-García, V., Calvo, L., Suárez-Seoane, S., & Marcos, E. (2023). Remote sensing advances in fire science: From fire predictors to post-fire monitoring. *Remote Sensing, 15*(20), Article 4930. https://doi.org/10.3390/rs15204930

Flannigan, M. D., Krawchuk, M. A., de Groot, W. J., Wotton, B. M., & Gowman, L. M. (2009). Implications of changing climate for global wildland fire. *International Journal of Wildland Fire, 18*(5), 483–507. https://doi.org/10.1071/WF08187

Foody, G. M. (2002). Status of land cover classification accuracy assessment. *Remote Sensing of Environment, 80*(1), 185–201. https://doi.org/10.1016/S0034-4257(01)00295-4

Franquesa, M., Vanderhoof, M. K., Stavrakoudis, D., Gitas, I. Z., Roteta, E., Padilla, M., & Chuvieco, E. (2018). Development of a standard database of reference sites for validating global burned area products. *Earth System Science Data, 10*(4), 2061–2076.

Gao, B. C. (1996). NDWI—A normalized difference water index for remote sensing of vegetation liquid water from space. *Remote Sensing of Environment, 58*(3), 257–266. https://doi.org/10.1016/S0034-4257(96)00067-3

Gibson, R., Danaher, T., Hehir, W., & Collins, L. (2020). A remote sensing approach to mapping fire severity in south-eastern Australia using Sentinel-2 and Random Forest. *Remote Sensing of Environment, 240,* Article 111702. https://doi.org/10.1016/j.rse.2020.111702

Gündüz, H. İ., Torun, A. T., & Gezgin, C. (2025). Post-fire burned area detection using machine learning and burn severity classification with spectral indices in İzmir: A SHAP-driven XAI approach. *Fire, 8*(4), Article 121. https://doi.org/10.3390/fire8040121

International Union for Conservation of Nature. (2022). *Forest landscape restoration*. https://www.iucn.org/our-work/topic/forest-landscape-restoration

Jolly, W. M., Cochrane, M. A., Freeborn, P. H., Holden, Z. A., Brown, T. J., Williamson, G. J., & Bowman, D. M. J. S. (2015). Climate-induced variations in global wildfire danger from 1979 to 2013. *Nature Communications, 6,* Article 7537. https://doi.org/10.1038/ncomms8537

Keeley, J. E. (2009). Fire intensity, fire severity and burn severity: A brief review and suggested usage. *International Journal of Wildland Fire, 18*, 116–126. https://doi.org/10.1071/WF07049

Li, J., & Roy, D. P. (2017). A global analysis of Sentinel-2A, Sentinel-2B and Landsat-8 data revisit intervals and implications for terrestrial monitoring. *Remote Sensing, 9*(9), Article 902. https://doi.org/10.3390/rs9090902

McFeeters, S. K. (1996). The use of the normalized difference water index (NDWI) in the delineation of open water features. *International Journal of Remote Sensing, 17*(7), 1425–1432. https://doi.org/10.1080/01431169608948714

Miller, J. D., & Thode, A. E. (2007). Quantifying burn severity in a heterogeneous landscape with a relative version of the delta normalized burn ratio (dNBR). *Remote Sensing of Environment, 109*(1), 66–80. https://doi.org/10.1016/j.rse.2006.12.006

NASA. (2025, May 28). *Wildfires and climate change*. NASA Science. https://science.nasa.gov/earth/explore/wildfires-and-climate-change/

Otsu, N. (1979). A threshold selection method from gray-level histograms. *IEEE Transactions on Systems, Man, and Cybernetics, 9*(1), 62–66. https://doi.org/10.1109/TSMC.1979.4310076

Park, C. Y., Takahashi, K., Li, F., Takakura, J., Fujimori, S., Hasegawa, T., Ito, A., Lee, D. K., & Thiery, W. (2023). Impact of climate and socioeconomic changes on fire carbon emissions in the future. *Global Environmental Change, 82,* Article 102667. https://doi.org/10.1016/j.gloenvcha.2023.102667

Parks, S. A., Dillon, G. K., & Miller, C. (2014). A new metric for quantifying burn severity: The relativized burn ratio. *Remote Sensing, 6*(3), 1827–1844. https://doi.org/10.3390/rs6031827

Pausas, J. G., Llovet, J., Rodrigo, A., & Vallejo, V. R. (2008). Are wildfires a disaster in the Mediterranean basin? *International Journal of Wildland Fire, 17,* 713–723. https://doi.org/10.1071/WF07151

Reichstein, M., Camps-Valls, G., Stevens, B., Jung, M., Denzler, J., Carvalhais, N., & Prabhat. (2019). Deep learning and process understanding for data-driven Earth system science. *Nature, 566,* 195–204. https://doi.org/10.1038/s41586-019-0912-1

Stehman, S. V. (2009). Sampling designs for accuracy assessment of land cover. *International Journal of Remote Sensing*, *30*(20), 5243–5272. https://doi.org/10.1080/01431160903131000

Tucker, C. J. (1979). Red and photographic infrared linear combinations for monitoring vegetation. *Remote Sensing of Environment, 8(2),* 127–150. https://doi.org/10.1016/0034-4257(79)90013-0

Turco, M., Rosa-Cánovas, J. J., Bedia, J., Jerez, S., Montávez, J. P., Llasat, M. C., & Provenzale, A. (2018). Exacerbated fires in Mediterranean Europe due to anthropogenic warming projected with non-stationary climate-fire models. *Nature Communications, 9,* Article 3821. https://doi.org/10.1038/s41467-018-06358-z

U.S. Department of Agriculture. (2023, January 19). *Biden-Harris Administration Launches New Efforts to Address the Wildfire Crisis*. https://www.usda.gov/about-usda/news/press-releases/2023/01/19/biden-harris-administration-launches-new-efforts-address-wildfire-crisis

Veraverbeke, S., Lhermitte, S., Verstraeten, W. W., & Goossens, R. (2012). Assessment of fire history with Landsat sensors. *Remote Sensing of Environment, 116,* 85–99. https://doi.org/10.1016/j.rse.2011.05.003

Wilson, E. O., & Peter, F. M. (Eds.). (1988). *Biodiversity*. National Academies Press.

Younger, K., Smith, A., & Johnson, R. (2024). Global trends in wildfire frequency and intensity: Implications for ecosystem management. *Fire Ecology, 20(1),* 1–18.